Monatshefte für Chemie - Chemical Monthly (2019) 150:871–875
https://doi.org/10.1007/s00706-019-2381-5

ORIGINAL PAPER

Synthesis, characterization, and POM-protein interactions of a Fe-substituted Krebs-type Sandwich-tungstoantimonate

Elias Tanuhadi[1] · **Ioannis Kampatsikas**[1] · **Gerald Giester**[2] · **Annette Rompel**[1]

Received: 23 December 2018 / Accepted: 25 January 2019 / Published online: 29 April 2019

Abstract

The novel iron-substituted Krebs-type polyoxotungstate $(C_{12}N_4H_{11})_4Na_2H_5[(Fe(H_2O)_3)_2((FeO_2)_{0.5}(WO_2)_{0.5})_2(\beta\text{-}SbW_9O_{33})_2]$ (**Fe-1**) has been synthesized using *ortho*-phenylenediamine (opda) as a precursor for the in situ formation of the counter cation 2,3-diaminophenazinium $(C_{12}N_4H_{11})^+$ (2,3-DAP). **Fe-1** has been thoroughly characterized in the solid state by single-crystal X-ray diffraction (SXRD), powder X-ray diffraction (PXRD), IR spectroscopy, and elemental analysis as well as in solution by UV–Vis spectroscopy. The crystal structure of **Fe-1** reveals π–π-interactions between the aromatic systems of the unconventional 2,3-DAP counter cation. POM-protein interaction studies using SDS-PAGE revealed a non-proteolytic behavior of **Fe-1** towards Human Serum Albumin (HSA) as a model protein.

Graphical abstract

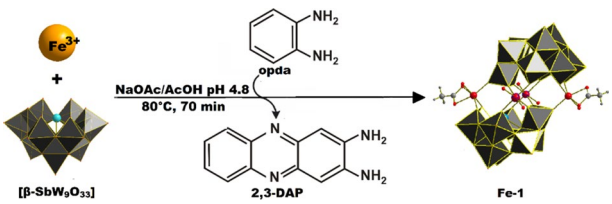

Keywords Sandwich polyoxometalates · Crystal structure · Proteins · Bioinorganic chemistry · Tungstoantimonates

Introduction

Polyoxometalates (POMs) [1] represent a broad class of anionic clusters, which are composed of metal ions in high oxidation states and linked by oxygen atoms resulting in a vast variety of unique structures. Depending on their size, charge, and composition, POM frameworks exhibit numerous different properties opening potential applications in different research fields of catalysis [2], materials science [3], and biological chemistry [4, 5] including protein crystallography [6, 7].

Among the POM family, transition metal substituted POMs (TMSPs) represent the largest group, mainly counting the subgroup of Sandwich-type POMs. Sandwich-type POMs, which are generally composed of two lacunary building blocks linked by a belt of heteroatoms, can be further divided into various subgroups, among them the Krebs-archetype.

Dedicated to Prof. Dr. Heinz Falk on the occasion of his 80th birthday.

Electronic supplementary material The online version of this article (https://doi.org/10.1007/s00706-019-2381-5) contains supplementary material, which is available to authorized users.

✉ Annette Rompel
annette.rompel@univie.ac.at
http://www.bpc.univie.ac.at

[1] Universität Wien, Fakultät für Chemie, Institut für Biophysikalische Chemie, Althanstraße 14, 1090 Wien, Austria

[2] Universität Wien, Fakultät für Geowissenschaften, Geographie und Astronomie, Institut für Mineralogie und Kristallographie, Althanstraße 14, 1090 Wien, Austria

Krebs-type POMs comprise two lone-pair containing β-Keggin lacunary fragments, e.g. $[\beta\text{-Sb(III)}W_9O_{33}]^{9-}$ [8]. The first representatives of the Krebs-archetype with the general formula $[M_2(H_2O)_6(WO_2)_2(\beta\text{-}SbW_9O_{33})_2]^{(14-2n)-}$ ($M = Fe^{3+}$, Co^{2+}, Mn^{2+}, Ni^{2+}) were reported by Krebs and co-workers in 1997 [8], exhibiting considerable importance in the fields of both homo- and heterogeneous catalysis [9]. The use of this archetype for the synthesis of new hexagon-type Sandwich POM compounds has recently been reported [10]. As Krebs-type POMs comprise free accessible metal centers, the natural ligand-binding interactions between protein side chains and the peripheral metal centers may be of interest for POM-assisted protein crystallography [11].

Inspired by the use of opda as a precursor for the in situ generation of the unconventional 2,3-DAP counter cation, the novel iron-substituted Krebs-type Sandwich POM $(C_{12}N_4H_{11})_4Na_2H_5[(Fe(H_2O)_3)_2((FeO_2)_{0.5}(WO_2)_{0.5})_2(\beta\text{-}SbW_9O_{33})_2]$ (**Fe-1**) has been prepared. Herein, we report on the synthesis and thorough characterization of the novel Fe-substituted Krebs-type Sandwich tungstoantimonate **Fe-1**. Regarding the scarce number of studies on the POM-protein interactions of the Krebs-POM archetype [10] and the potential use of non-proteolytic POM clusters as additives in POM-assisted protein crystallography, the POM-protein interactions of **Fe-1** with Human serum albumin (HSA) as a model protein were investigated using SDS-PAGE to assess whether **Fe-1** shows any proteolytic activity towards HSA.

Results and discussion

Synthesis of Fe-1

An aqueous solution of $Na_9[SbW_9O_{33}]$ contains a mixture of $[\alpha\text{-}SbW_9O_{33}]$ and $[\beta\text{-}SbW_9O_{33}]$ in equilibrium. It is well documented that the latter species $[\beta\text{-}SbW_9O_{33}]$ dominates the equilibrium at pH values lower than 6.0 [8]. As a matter of fact, the reaction was carried out in an acetate buffer at pH 4.8. Upon addition of opda to a warm aqueous acidic reaction mixture of $Na_9[SbW_9O_{33}]$ and $FeCl_3$, the initially yellow solution gradually turned dark red indicating the oxidation of opda to 2,3-diaminophenazine (2,3-DAP) catalyzed by the in situ formed **Fe-1** Krebs-POM. Cooling of the reaction mixture to room temperature resulted in the formation of dark red crystal plates consisting of polyanion **Fe-1** (Scheme 1).

Crystal structure of Fe-1

Single crystal X-ray diffraction (SXRD) studies were performed on **Fe-1** revealing a Krebs-type structure which crystallizes in the triclinic space group **P-1**. The crystal structure of **Fe-1** exhibits two $[\beta\text{-}SbW_9O_{33}]$ lacunary species linked by two Fe(III) metal centers at the peripheral sites and two W(VI) centers which show a 50:50 disorder with Fe(III) at the inner position of the linking belt. Regarding the synthetic conditions of **Fe-1**, which include the use of an acidic buffer (pH = 4.8), the disorder with tungsten is in accordance with the results for the disordered alpha-arsenotungstate compounds observed at lower pH values, reported by Kortz et al. in 2001 [12] as well as the disordered Krebs-type tungstoantimonates recently reported by our group [10]. The peripheral iron centers exhibit a distorted octahedral coordination environment with one acetate ligand and one H_2O molecule coordinated to the metal center and Fe–O bond lengths ranging from 1.9271(1) at the inner site of the belt to 2.139(1) Å between the peripheral iron centers and the H_2O ligand at the peripheral belt positions (Fig. 1).

Besides SXRD, **Fe-1** was also characterized in the solid state by powder X-ray diffraction (PXRD) (Fig. S1), ATR-IR spectroscopy (Fig. 2), and elemental analysis.

Scheme 1

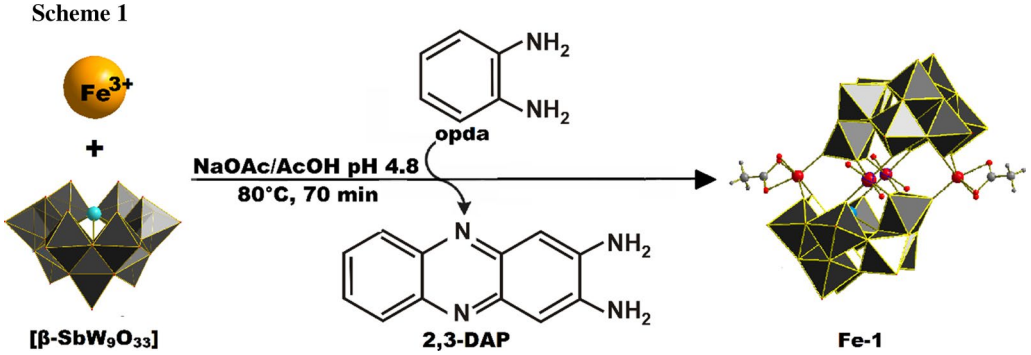

Scheme 1 Structure and synthesis of **Fe-1**. The synthesis starts from the $[\beta\text{-}SbW_9O_{33}]$ unit and $FeCl_3$. Catalytic oxidation of opda by the in situ formed **Fe-1** anion leads to formation of 2,3-diaminophenazinium (2,3-DAP) which acts as a counteraction for **Fe-1**. Counter cations are omitted for clarity. Color legend: WO_6, grey; Sb, light blue; Fe, light orange; disordered Fe/W centers, light orange with dark blue stripes; O_t, red

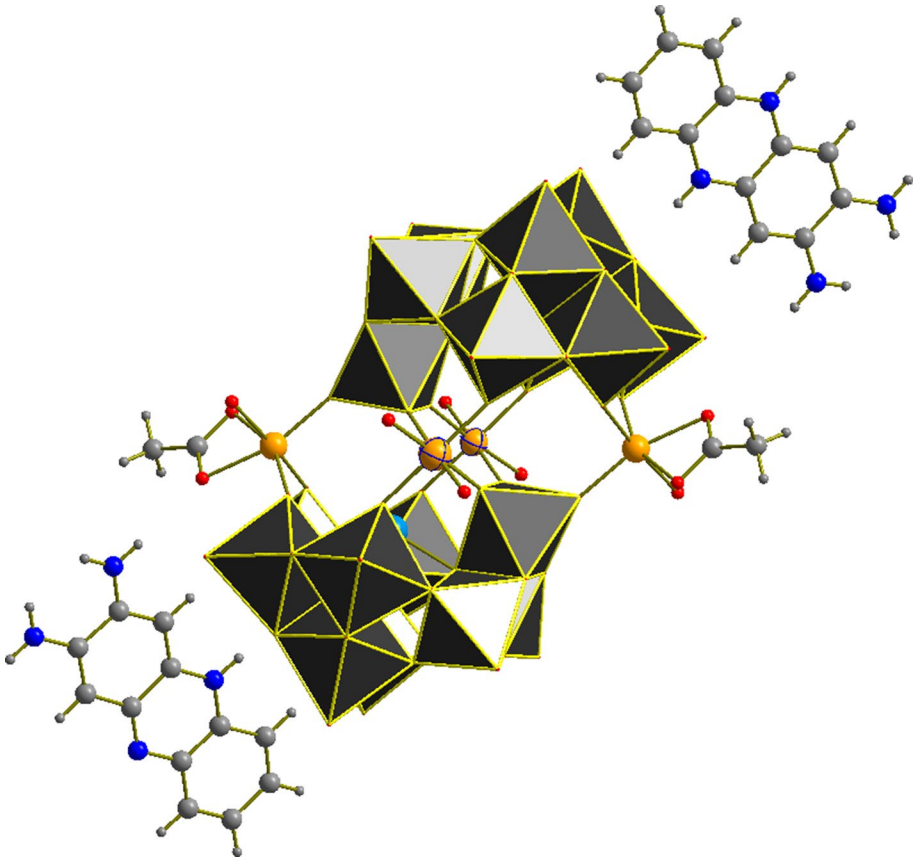

Fig. 1 Polyhedral representation of **Fe-1**. WO_6, grey; Sb, light blue; Fe, light orange; disordered Fe/W centers, light orange with dark blue stripes; O_t, red; C, light grey; N, blue

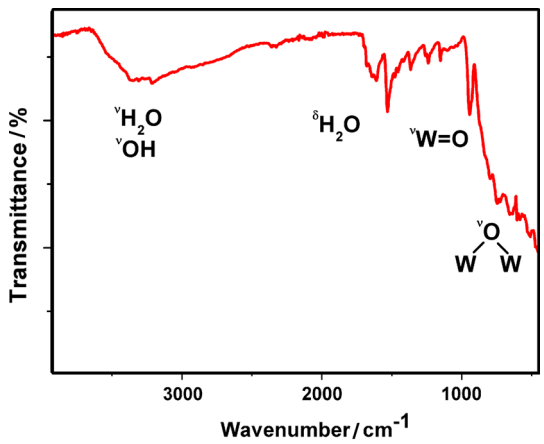

Fig. 2 IR spectrum of $(C_{12}N_4H_{11})_4Na_2H_5[(Fe(H_2O)_3)_2((FeO_2)_{0.5}(WO_2)_{0.5})_2(\beta\text{-}SbW_9O_{33})_2]$ (**Fe-1**)

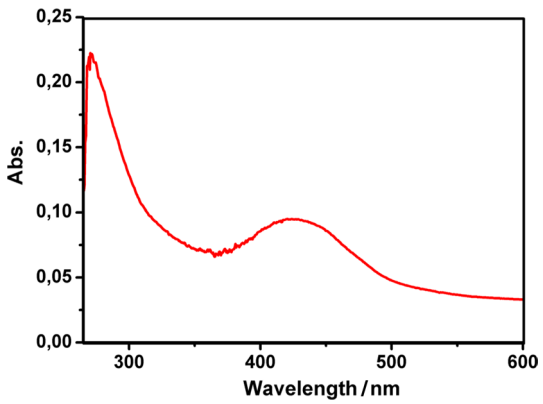

Fig. 3 UV–Vis-spectrum of **Fe-1** (5×10^{-6} M) in 10 mM NaOAc buffer pH 5.5 showing typical O→W ligand—to—metal charge-transfer (271 nm) and aromatic transitions (423 nm)

UV–Vis spectrum of Fe-1

The UV–Vis spectrum of **Fe-1** exhibits two major peaks, one at 271 nm corresponding to the $p\pi(O_b) \rightarrow d\pi^*(W)$ ligand-to-metal charge-transfer transition typical for the Keggin-type framework [13], whereas a second absorption maximum at 423 nm can be attributed to the aromatic transitions of the 2,3-DAP counter cations present in the structure [14] (Fig. 3).

POM-protein interactions

Considering the known catalytic activity of Fe(III) as a Lewis acid, the POM-protein interactions of the peripheral Fe(III) metal centers of **Fe-1** with human serum albumin

(HSA) as a model protein were investigated to assess whether **Fe-1** exhibits any proteolytic activity. SDS-PAGE was performed on reaction mixtures of HSA and **Fe-1** in a NaOAc buffer [10 mM] pH 5.5 to ensure a stable more accessible acidic conformation of the model protein [15]. The results revealed no hydrolytic activity of **Fe-1** towards the peptide bonds of the model protein even at 65 °C and 100-fold excess of the POM compound indicated by intact protein bands at 66 kDa (Fig. 4). This is in good accordance with our previous results reported for the isostructural manganese- and zinc-substituted DAP–POM derivatives [10].

Conclusion

In conclusion, the synthetic pathway presented in this work may open new perspectives for the preparation of novel Krebs-POM archetypes exhibiting unconventional counter cations. The interactions of the Krebs-POM compound **Fe-1** with HSA as a model protein have been investigated and the non-proteolytic behavior of **Fe-1** may be interesting for further POM-protein interaction studies ultimately perhaps opening novel perspectives in the field of POM-assisted protein crystallography.

Experimental

All reagents were obtained commercially from Aldrich, of high-purity grade and were used as purchased without further purification. $Na_9[B\text{-}\alpha\text{-}SbW_9O_{33}]$ was prepared according to the literature procedure reported by Bösing et al. [8]. X-ray intensity data were measured on a Bruker X8 APEX2 diffractometer equipped with a multilayer monochromator, Mo K/α INCOATEC micro focus sealed tube and Oxford cooling device. The following software was used: Bruker SAINT software package [16] using a narrow-frame algorithm for frame integration, OLEX2 [17] for structure solution, refinement, molecular diagrams and graphical user-interface, Shelxle [18] for refinement and graphical user-interface SHELXS-2013 [19] for structure solution, SHELXL-2013 [20] for refinement. Experimental data and the CCDC-Code are provided in Table S1. Crystal data, data collection parameters, and structure refinement details are given in Tables S2 and S3 of the electronic supporting information. X-ray powder diffraction measurements were performed on a Bruker D8 ADVANCE diffractometer, Cu Kα radiation, $\lambda = 1.54{,}056$ Å, LYNXEYE silicon strip detector and SolX energy dispersive detector, variable slit aperture with 12 mm, $5° \leq 2\theta \leq 40°$. Attenuated total reflection Fourier-transform Infrared Spectroscopy: all spectra were recorded on a Bruker Tensor 27 IR Spectrometer equipped with a single-reflection diamond-ATR unit. Frequencies are given in cm^{-1}, intensities denoted as w = weak, m = medium, s = strong. Elemental analysis (C, H, N, O) was performed at Mikroanalytisches Laboratorium, Fakultät für Chemie, Universität Wien using the 2400 CHN Elemental Analyzer and the EA 3000, respectively. UV–Vis spectra were collected on a Shimadzu UV 1800 spectrophotometer. The spectra were recorded in 10 mM NaOAc buffer pH 5.5. SDS-PAGE was performed according to a standard procedure [21] using Precision Plus Protein Standard Dual Color (Bio-Rad) as molecular weight marker. Samples were applied to 14% polyacrylamide gels under reducing conditions. The sample amount loaded onto the gel was 5 µg. Gels were stained with Coomassie Brilliant Blue. Imaging of the gels was applied with Gel Doc™ XR of BIO-RAD. Human serum albumin (HSA) (5 µg) was mixed with 1, 10, and 100 equivalents of

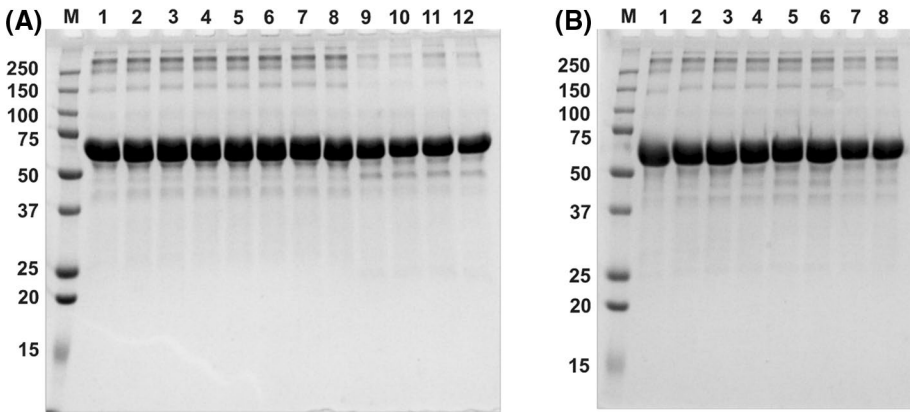

Fig. 4 HSA incubated with **Fe-1** for 30 min at 20 °C (1–4), at 37 °C (5–8), and at 65 °C (9–12). **1)** 5 µg HSA without **Fe-1**, **2)** 1:1 HSA:POM, **3)** 1:10 HSA:POM, **4)** 1:100 HSA:POM., **5)** 5 µg HSA without **Fe-1**, **6)** 1:1 HSA:POM, **7)** 1:10 HSA:POM, **8)** 1:100 HSA:POM, **9)** 5 µg HSA without **Fe-1**, **10)** 1:1 HSA:POM, **11)** 1:10 HSA:POM, **12)** 1:100 HSA:POM in NaOAc buffer [10 mM] 5.5 pH **A)** HSA with **Fe-1** after 30 min **B)** HSA with **Fe-1** after 3 days

Fe-1 in 10 mM NaOAc buffer pH 5.5 and incubated at three different temperatures (20, 37, and 65 ºC).

$(C_{12}N_4H_{11})_4Na_2H_5[(Fe(H_2O)_3)_2((FeO_2)_{0.5}(WO_2)_{0.5})_2(\beta\text{-}SbW_9O_{33})_2]$ (*Fe-1*) To a stirred solution of 215 mg $Na_9[B\text{-}\alpha\text{-}SbW_9O_{33}]$ (0.05 mmol) in 20 cm^3 aqueous sodium acetate buffer (0.5 M NaOAc/AcOH, pH 4.8), 81 mg $FeCl_3 \cdot 6H_2O$ (0.3 mmol) was added. The resulting orange reaction mixture was stirred at 70 °C for 10 min. o*rtho*-Phenylenediamine (opda, 21 mg, 0.2 mmol) was added to the reaction solution and the mixture was stirred for further 60 min at 85 °C. A color change from orange to dark red over the time period of 60 min was noticed. Dark red crystal plates of **Fe-1** were obtained upon cooling the filtered reaction mixture to room temperature and further evaporation at 18 °C gave a total yield of 60% based on W after 3 days. IR (ATR): $\tilde{\nu}$ = 3363.4 (w), 3260.6 (w), 1635.1 (m), 1509.2 (m), 1400.4 (m), 1233.4 (s), 1152.1 (s), 935.8 (s), 744.5 (s) cm^{-1}.

Acknowledgements Open access funding provided by Austrian Science Fund (FWF). We gratefully acknowledge the Austrian Science Fund FWF (P27534) as well as the University of Vienna for financial support. E.T. and A.R. acknowledge the University of Vienna for awarding an Uni:docs fellowship to Elias Tanuhadi. Lastly, the authors wish to thank Nadiia Gumerova, PhD, Dipl.-Ing. Matthias Pretzler, Dr. Joscha Breibeck, Emir Al-Sayed, MSc and Ing. Alexander Roller for valuable discussions concerning this work.

References

1. Pope MT (1983) Heteropoly and Isopoly oxometalates. Springer-Verlag, Berlin
2. Wang S, Yang GY (2015) Chem Rev 11:4893
3. Kastner K, Kibler AJ, Karjalainen E, Fernandes JA, Sans V, Newton GN (2017) J Mater Chem A 5:11577
4. Bijelic A, Aureliano M, Rompel A (2018) Chem Commun 54:1153
5. Bijelic A, Aureliano M, Rompel A (2019) Angew Chem Int Ed 58:2980
6. Bijelic A, Rompel A (2017) Acc Chem Res 50:1441
7. Bijelic A, Rompel A (2015) Coord Chem Rev 299:22
8. Bösing M, Loose I, Pohlmann H, Krebs B (1997) Chem Eur J 3:1232
9. Bösing M, Nöh A, Loose I, Krebs B (1998) J Am Chem Soc 120:7252
10. Tanuhadi E, Roller A, Giester G, Kampatsikas I, Rompel A (2018) Dalton Trans 47:15651
11. Boggon TJ, Shapiro L (2000) Structure 8:143
12. Kortz U, Al-Kassem NK, Savelieff MG, Al Kadi NA, Sadakane M (2001) Inorg Chem 40:4742
13. Bi L, Li B, Wu L, Bao W (2009) Inorg Chim Acta 362:3309
14. Zhou P, Liu H, Chen S, Lucia L, Zhan H (2011) Molbank 2011:M730
15. Dockal M, Carter DC, Rüker F (2000) J Biol Chem 275:3042
16. Bruker SAINT v7.68A Copyright © 2005–2016 Bruker AXS
17. Dolomanov OV, Bourhis LJ, Gildea RJ, Howard JAK, Puschmann H (2009) J Appl Cryst 42:339
18. Huebschle CB, Sheldrick GM, Dittrich B (2011) J Appl Cryst 44:1281
19. Sheldrick GM (1996) SHELXS. University of Göttingen, Göttingen, Germany
20. Sheldrick GM (1996) SHELXL. University of Göttingen, Göttingen, Germany
21. Laemmli UK (1970) Nature 227:680